I&EC research
Industrial & Engineering Chemistry Research

pubs.acs.org/IECR
Article

Highly Selective CO_2/CH_4 Membranes Based on Ethanolamine Ionic Liquids

Murilo Leite Alcantara,* Gerlon de Almeida Ribeiro Oliveira, Luciano Morais Lião, Alfredo Ortiz, and Silvana Mattedi

Cite This: *Ind. Eng. Chem. Res.* 2024, 63, 8306−8318

ABSTRACT: In the pursuit of advanced carbon capture methods, ionic liquid (IL)-based membranes have emerged as promising materials for CO_2 separation due to their high permeation and selectivity. This research focuses on the development of composite membranes with highly CO_2 selective ethanolamine-based ionic liquids and poly(vinyl alcohol) (PVA). ILs and membranes were characterized by water content, FT-IR, ^1H, and ^{13}C NMR. The addition of ethanolamine-based ILs and stream humidification promoted an outstanding increase of PVA membranes' CO_2 permeability and CO_2/CH_4 selectivity of 53× and 36×, respectively. Effects of transmembrane pressure (1.0 to 3.0 barg), temperature (313.15 to 343.15 K), and CO_2:CH_4 ratio (10 to 40%) were studied. Effects of IL's cations and alkyl chain length (anion) on CO_2 separation performance were studied via the production of PVA membranes with seven ethanolamine-based ILs. CO_2 permeabilities up to 209 barrer and selectivities up to 241 were obtained. The comparison of these membranes with some of the most promising materials in the literature indicates that the ethanolamine-based ILs + PVA membranes have moderate CO_2 permeabilities, associated with outstanding CO_2/CH_4 selectivities.

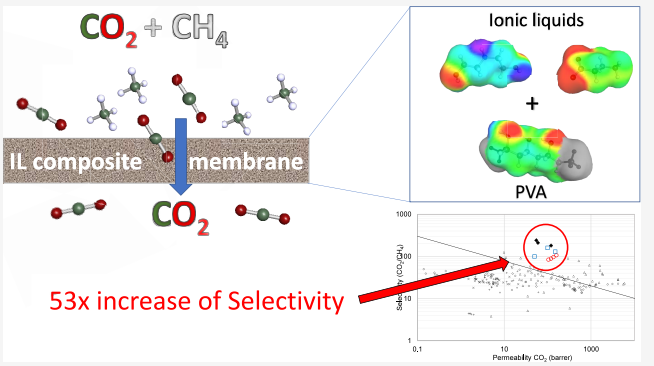

1. INTRODUCTION

The rise in atmospheric carbon dioxide (CO_2) levels, largely attributed to human activities, such as burning fossil fuels, has resulted in elevated global temperatures. This change triggers more frequent severe weather events, escalating sea levels, and has detrimental impacts on human health and ecosystems. The surging CO_2 concentration over recent years[1] has emphasized the pressing need for novel technologies to address this crisis.[2]

Carbon capture solutions prioritize the separation of CO_2 before its atmospheric release, thereby lessening its ecological consequences and aiding the transition to a sustainable, low-carbon future. Although chemical absorption remains the dominant method for CO_2 separation, alternatives like membrane separation potentially offer environmental advantages, energy efficiency, and scalability.[3−5]

A significant challenge in the evolution of membrane separation for industrial use lies in choosing the appropriate membranes. Such a material ought to be selective, permeable, and durable under the intended operational conditions.[4] The recent literature[6,7] indicates that integrating certain ionic liquids (ILs) can enhance the gas permeation capabilities of membranes. Membranes with IL content tend to demonstrate superior CO_2 permeabilities and selectivities, albeit sometimes at the cost of mechanical integrity.[8,9]

Ionic liquids are ionic compounds with low melting points, at least under 373.15 K.[10] The ions in ILs form stable Coulomb and ionic bonds, accounting for their high thermal resilience, elevated viscosity, and minimal vapor pressure. Ionic liquids can be integrated into membrane separation via methods such as supported ionic liquid membranes (SILMs), polymerized ionic liquids (PILs), ion-gel membranes, and IL composite membranes. The last one has the advantage of resisting to high-pressure differentials; however, it requires the choice of IL-polymer pairing with suitable compatibility to ensure optimal interactions.[7]

Some of the most studied ionic liquids are composed of imidazolium, pyridinium, and quaternary ammonium cations. These ions, when combined with polar CO_2 selective anions, such as cyanide ([CN]) and acetate ([Ac]), may facilitate the development of feasible IL-based processes for carbon capture purposes.[11,12] However, the synthesis of these ionic liquids often involves high costs and presents moderate to significant

Received: December 20, 2023
Revised: April 17, 2024
Accepted: April 17, 2024
Published: April 26, 2024

https://doi.org/10.1021/acs.iecr.3c04533
Ind. Eng. Chem. Res. 2024, 63, 8306−8318

ecotoxicological risks.[13,14] In contrast, ionic liquids featuring hydroxyethylammonium cations and anions derived from carboxylic acids offer a cost-effective and less toxic alternative.[15] They demonstrate enhanced solubility in CO_2 and superior CO_2/CH_4 selectivity when compared to certain imidazolium or pyridinium-based counterparts.[16,17] Recent developments[18] in ethanolamine-based composite membranes have shown them to possess remarkable CO_2/CH_4 selectivity and satisfactory CO_2 permeability, positioning them as notable contenders among CO_2 selective ionic liquids.

The poly(vinyl alcohol) (PVA) polymer has proven effective in supporting carriers in high-performing CO_2-facilitated transport membranes.[19] The PVA + [m-2HEA][Pr] composition, in particular, displayed promising results for CO_2/N_2 and CO_2/CH_4 separation.[18] Nonetheless, the transport mechanisms and effects of variables such as temperature, pressure, and humidification treatment on other ethanolamine-based ILs remain underexplored. This study's main goal is to investigate the application of ethanolamine-based ILs and PVA membranes to separate CO_2 from methane.

2. MATERIALS AND METHODS

All materials, characterizations, experiments, and calculus performed within this study were presented in this section.

2.1. Selection and Synthesis. *2.1.1. Ionic Liquids.* Seven ethanolamine-based ILs were investigated in this study. In the first part, only *N*-methyl-2-hydroxyethylammonium propionate [m-2HEA][Pr] was applied. Later, six ethanolamine-based ILs were synthesized based on $[2HEA]^+$ (2-hydroxyethylammonium) and $[BHEA]^+$ (bis-2-hydroxyethylammonium) cations. The anions' structures were designed from carboxylic acids of varied carbon chains, ranging from two carbons ($[Ac]^-$) to four (Butanoate, $[Bu]^-$). This led to the formation of the following ionic liquids: bis-2-hydroxyethylammonium acetate [BHEA][Ac], bis-2-hydroxyethylammonium propionate [BHEA][Pr], bis-2-hydroxyethylammonium butanoate [BHEA][Bu], 2-hydroxyethylammonium acetate [2HEA][Ac], 2-hydroxyethylammonium propionate [2HEA][Pr], and 2-hydroxyethylammonium butanoate [2HEA][Bu].

All ILs were synthesized under controlled conditions by neutralizing equimolar amounts of carboxylic acids with amines. Precursors with mass purities of 99% or greater were sourced from Sigma-Aldrich (see Supporting Information, S1 for details). The synthesis involved amine neutralization using carboxylic acid in a three-necked glass reactor. Before the reaction, the flask was purged with nitrogen and placed within a thermal bath set at 283.1 K. The process began with the introduction of a measured quantity of the amine followed by a gradual addition of the carboxylic acid. Any residual solvent was eliminated using rotary evaporation at 333.15 K for 24 h under a mild vacuum (20 mbar), yielding a viscous end product. This synthesis procedure, known to yield high-purity ILs with comparable precursors, has been documented in previous studies.[17,18] The molecular structures of the crafted ILs were verified using NMR spectroscopy (details in the Supporting Information, S1).

2.1.2. Membranes. All membranes were prepared by the solvent evaporation technique[5] from a solution of water, PVA, and a selected IL. In brief, a weighted amount of IL was added to a 5% wt. aqueous solution of PVA and mixed at 20 °C over 1 h in a closed flask. Then, the solution was kept steady (without stirring) over 6h to remove bubbles formed during the mixing step. Then, bubble-free solutions were spread over a Petri dish and left to air-dry at room temperature for over 48 h.

The 5% wt. PVA solution was prepared by dissolving PVA pellets in water at 90 °C in a round-bottom flask fitted with a magnetic stirrer. Subsequently, an exact amount of IL was added to the PVA solution at a proportion of 40 wt % % of IL and 60 wt % % of PVA. The amount of IL was calculated by reducing its water content. The combined solution was stirred for 30 min at room temperature within a sealed flask and was then left undisturbed for at least 12 h until a minimal amount of bubbles were observed.

About 10 g of the IL:PVA solution was evenly spread on a 150 mm diameter Teflon Petri dish. Subsequently, the plate was left exposed to ambient conditions (293−298 K) for 48 h to promote gradual evaporation of the solvent, water.

Some membranes were exposed to 12 h vacuum treatment at 3 mbar and 303.15 K to remove further excess of water. The majority of the membranes under this study were not exposed to vacuum treatment for reasons later explained within section 3.3.

2.2. Characterization. *2.2.1. Induced Charge Density Profile.* The ILs' induced charge density profiles and molecular structure were estimated through the HF-TZVP level of theory. In brief, this approach performs a geometrical and electronic energy minimization, which results in 3D molecular structures and charge density profiles of investigated species. This method was reported to produce a high representation of species' charge density with a reasonably low computational cost.[20] This information was used to evaluate the IL's polarity from a qualitative perspective only. The separated ions' charge distribution is converted into a 2D graph called the sigma profile, which could be later used for some properties and the ILs' activity coefficient functions via predictive models such as COSMO-SAC.

2.2.2. Water Content. Ethanolamine-based ILs have a well-documented propensity for hygroscopy.[21] As a result, it was imperative to measure their water content to ensure that minimal water absorption occurred during the rotary evaporation process post-IL synthesis. This assessment was executed using a Metrohm 831 Karl Fischer coulometer titrator with three repeated measurements.

2.2.3. Nuclear Magnetic Resonance (NMR). Both ^1H and ^{13}C NMR analyses of pure ILs and IL composite membranes were performed to evaluate the species' structures. The ^1H NMR spectra also allowed for the estimation of the purity of the ILs via area percentage or the assay method. The spectra were acquired at 20 °C on a Bruker Avance III 500 spectrometer operating at 11.75 T. DMSO-d_6 was used as a solvent for the membrane samples, and D_2O was used as a solvent for the IL samples.

The acquisition parameters were as follows: 1 and 500 scans (NS), spectral windows (SW) of 25 and 284 ppm, acquisition times (AQ) of 2.62 and 0.92 s, and relaxation delays of 1 and 0.5 s for ^1H and ^{13}C, respectively. Both experiments were acquired with 64 000 points (TD). The results were analyzed by using the Bruker TopSpin software. ^1H and ^{13}C chemical shifts are given in δ (ppm) and related to the TMSP-d_4 signal at δ 0.00 as an internal reference.

^1H NMR was also employed to estimate the IL-to-PVA ratio in the newly fabricated membranes. This value was compared to the experimental weighted ratio of PVA and IL used to produce the IL/PVA solution; these ratios were expected to be close, as neither PVA nor IL is expected to be lost during

https://doi.org/10.1021/acs.iecr.3c04533
Ind. Eng. Chem. Res. 2024, 63, 8306−8318

membrane preparation.[1]H NMR can be utilized for quantitative analysis, as signal intensities are proportional to the molar concentrations of the respective substances. Quantitative NMR (qNMR) is advantageous due to its broad linearity range and accuracy, without necessitating specific reference substances.[22,23] For quantification, approximately 10.00 mg of membrane samples were dissolved in 600 μL of DMSO-d_6, while around 20.00 mg of the external standard, maleic acid, was weighed separately into a centrifuge tube and combined with 500 μL of D_2O. ILs were also assayed after dissolution of around 20.00 mg in 500 μL of D_2O. Upon complete dissolution through stirring, the solutions were transferred to 5 mm NMR tubes. Solutions were analyzed in triplicate. ^{1}H NMR experiments started 60 s after spectrometer shimming to ensure near-complete longitudinal relaxation, as determined by inversion recovery experiments. NMR signals not overlapping with impurities were chosen for quantification. Impurity overlapping was detected by the assessment of peak shape, by the variation of peak area in relation to the stoichiometry of the molecule, or by the presence of correlations not due to the analyte, in two-dimensional experiments.

2.2.4. Fourier Transform Infrared Spectroscopy (FT-IR). Fourier Transform Infrared (FT-IR) spectroscopy measurements were conducted with a Spectrum Two spectrometer (PerkinElmer), covering a wavelength range from 400 to 4000 cm^{-1}. Experiments were carried out in a temperature-controlled environment, approximately 290 K. Samples were prepared by spreading on a sapphire window utilizing the attenuated total reflection (ATR) technique at a resolution of 0.10 cm^{-1}. Spectra were derived from an average of 10 scans, aiming to elucidate the structural characteristics of the examined ionic liquids (ILs) and their composite membranes with PVA.

2.3. Gas Permeation Experiments. In brief, the gas experiments consist of preparing a permeation module in which the membranes were exposed to a CO_2/CH_4 stream under controlled conditions. Part of these gases permeate through the membrane and are sent for quantification with a gas chromatograph.

2.3.1. Gas Permeation Procedure. The prepared membranes were cut into circular shapes of roughly 8.2 cm diameter to fit the permeation modulus. The membrane thickness was measured at five distinct locations using a micrometer with a 0.01 μm resolution.

The membrane is then placed over a porous metallic support of stainless steel, and a Viton-O ring is placed over the membrane to avoid leakage. Thus, the membrane's upper chamber is placed, locked, and connected to the gas permeation module, as shown in Figure 1.

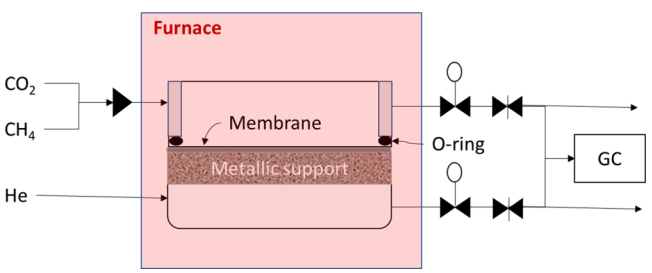

Figure 1. Sketch of the gas permeation modulus.

A CO_2:CH_4 blend is prepared by calibrated massflowmeters, connected to pure CO_2 and CH_4 gases acquired by White Martins (>99.9%). For the majority of this study, a proportion of 40:60 (CO_2:CH_4) was employed. The chambers' pressures are controlled by pressure transducers (Ashcroft GC-35, 0−8 bar) and needle valves. The bottom chamber was flowed with Helium to lead the gases that permeate through the membrane to the gas chromatograph. Both gas flow rates were set at 20 cm^3 (STP)/min.

To guarantee a stable isothermal environment, the membrane cell was stationed inside a furnace. The majority of the tests were executed at 303.15 K to replicate ambient gas separation conditions. Real-time evaluation of the gas compositions was performed by utilizing gas chromatography.

As is better explained within Section 3.2, stream humidification was applied to the majority of the performed experiments. For these tests, a cylindrical flask containing 200 mL of distilled water was set in the furnace. The CO_2:CH_4 blend was first directed through this flask to achieve humidification before its introduction to the upper chamber of the membrane cell.

Although the water percentage of these streams was not experimentally measured, it can be estimated given the known temperature and pressure and assuming that the streams reach water saturation. The theoretical cap on water absorption was determined by assuming a 100% humidity level. Typically, for the majority of tests, this value hovered around 2.5%, whose calculus can be found within the Supporting Information (S2). It is worth noting that the concentration of water was excluded from the permeability calculations.

2.3.2. Calculus Description. The membranes' permeation performances were evaluated by their permeabilities. This metric is correlated to the volume of gas that flows through a membrane given a certain thickness and pressure differential applied. Permeabilities can be calculated according to eq 1,

$$p_i = -10^{10}\frac{Q_{i.Perm} \times l_{memb}}{A_{memb} \times \Delta P_i} \quad (1)$$

in which p_i denotes the permeability of gas i in barrer units [10^{-10} cm^3_{STP} × cm/(cm^2 × s × cmHg), $Q_{i.Perm}$ is the volumetric flow rate of gas i through the membrane (cm^3_{STP}/s), l_{memb} is the membrane thickness (cm), A_{memb} stands for the effective permeation area (cm^2), and ΔP_i is the partial pressure differential of the species i across the membrane chamber (cmHg).

The effective permeation area, A_{memb}, was fixed (52.8 cm^2) for all experiments. The l_{memb} is derived as an average from five thickness measurements taken postexperiments, typically fluctuating between ∼50 and ∼80 μm. The transmembrane differential pressure, ΔP_i, is computed based on the partial pressures of each species in both chambers. These values were calculated by considering ideal gas behavior (Raoult and Dalton laws) and multiplying total pressure by the gas concentration. All gaseous concentrations were obtained by calibrated gas chromatograms of the permeate samples. For most trials, the concentrations of CO_2 and CH_4 within the sweep gas were quite low, not exceeding 3%.

All CO_2/CH_4 selectivities presented in this study are permselectivities (α_{CO_2/CH_4}) estimated by the ratio between the permeabilities of each gas, as shown in eq 2.

https://doi.org/10.1021/acs.iecr.3c04533
Ind. Eng. Chem. Res. 2024, 63, 8306−8318

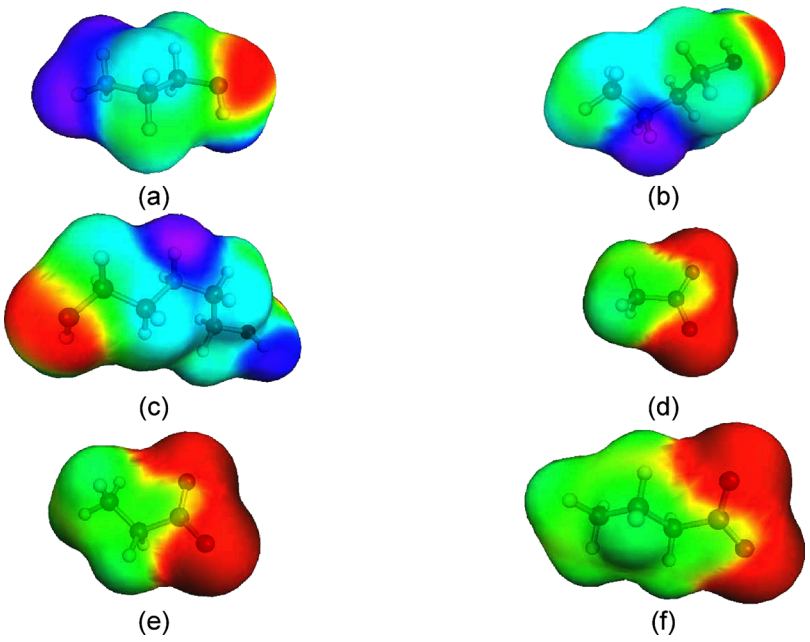

Figure 2. Molecular structure of all ions studied: cations (a) $[2HEA]^+$, (b) $[m\text{-}2HEA]^+$; and (c) $[BHEA]^+$; anions (d) $[Ac]^-$, (e) $[Pr]^-$, and (f) $[Bu]^-$.

$$\alpha_{a/b} = \frac{p_a}{p_b} \quad (2)$$

2.3.3. Gas Chromatography (GC). The concentrations of CO_2 and CH_4 in the gaseous streams were quantified by using gas chromatography. Real-time analysis of the gaseous stream compositions was performed with a Shimadzu Tracera GC-2010. This system features a Barrier Ionization Discharge (BID) detector, which has the sensitivity to detect concentrations down to the ppb level.

The GC is equipped with two columns selected depending on the analyzed component. The first column is a molecular sieve capillary column (SH/Rt/Molecular sieve 5A) used to analyze CH_4. The second column is a fused silica capillary column (Carboxen 1010 Plot) used to analyze CO_2.

The entirety of the GC analytical process spans 9 min. Throughout this duration, helium served as the carrier gas for both columns, maintained at a steadfast pressure of 4.5 bar.

3. RESULTS AND DISCUSSION

NMR and FT-IR spectroscopies and Karl Fischer titration were performed to identify and quantify the IL structures in the composite membranes. Next, the [m-2HEA][Pr] + PVA membrane was applied to CO_2/CH_4 permeation experiments under several conditions to evaluate the influence of the temperature, pressure, gas humidification, and gas composition. Finally, six ethanolamine-based ILs were added to the PVA matrix instead of the [m-2HEA][Pr] to evaluate the performance of IL composite membranes in CO_2/CH_4 separation. All membranes under study' performances were compared to the literature through Robeson's plot.

3.1. Ionic Liquid Characterization. *3.1.1. Induced Charge.* Figure 2 illustrates the induced charge density profile alongside the molecular structures of all of the ions. Negative charges are represented in blue, positive charges in red, and neutral charges in yellow. Notably, the induced charges of cations like $[2HEA]^+$, $[m\text{-}2HEA]^+$, and $[BHEA]^+$ predominantly display a blue color (indicative of negative charges), while anions exhibit a more pronounced red color ($[Ac]^-$, $[Pr]^-$, and $[Bu]^-$). The combination of these ions can form all of the ILs selected for this study.

By analysis of Figure 2, it is worth noting that $[2HEA]^+$ exhibited the most pronounced region of high negative charge densities, evident from its predominant blue charge concentration. The acetate anion presents the most concentrated electronegative charges of the anions considered, as it is evidenced by the reddish colors. Additional analysis of these species σ-profile, sites of interactions, and polarity can be found within the Supporting Information.

3.1.2. Karl Fischer Titration. Ethanolamine-based ionic liquids (ILs) are renowned for their pronounced water sorption capabilities.[21,24] It is essential to accurately determine the water content in the ILs, especially when formulating composite membranes with a specific 40 wt % ratio between the IL and PVA. Table 1 consolidates the average water content for all of the examined ethanolamine-based ILs. Although these ILs possess innate hygroscopic tendencies, they were synthesized by exhibiting remarkably low water contents.

Table 1. Water Contents and Purity of the ILs under Study

ionic liquid	water content[a] (wt % g_{water}/g)	cation/anion ratio	purity[b] (%)
[m-2HEA][Pr]	3.42 ± 0.16	1.03	95.8
[2HEA][Ac]	1.07 ± 0.05	0.98	86.1
[2HEA][Pr]	0.41 ± 0.03	1.00	98.5
[2HEA][Bu]	0.29 ± 0.01	1.01	98.8
[BHEA][Ac]	0.63 ± 0.02	1.01	90.8
[BHEA][Pr]	0.35 ± 0.03	1.00	93.0
[BHEA][Bu]	0.35 ± 0.01	0.97	94.9

[a]As mean ± expanded uncertainty, considering a normal error distribution, for the covering factor of 2 (k = 2, 95%). [b]Purity was estimated by calculating the percentage of area integration for impurities and analytes in the ^1H NMR spectra.

https://doi.org/10.1021/acs.iecr.3c04533
Ind. Eng. Chem. Res. 2024, 63, 8306−8318

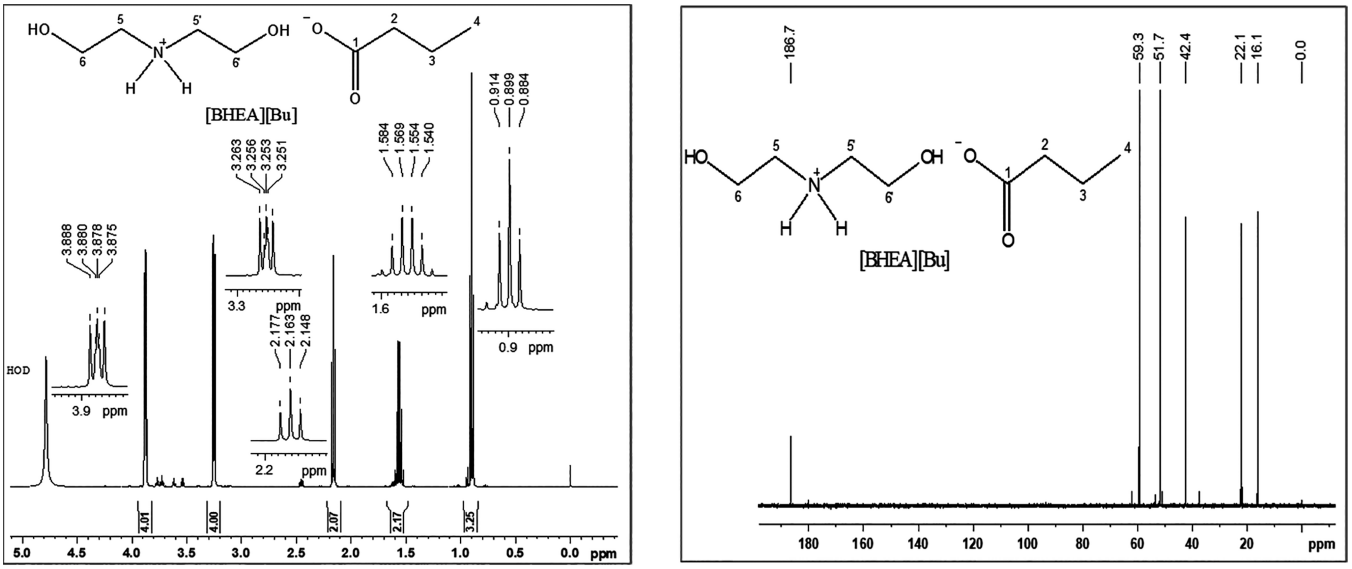

Figure 3. (a) ^{1}H NMR (500 MHz, D_2O) and (b) ^{13}C NMR (125 MHz, D_2O) spectra for [BHEA][Bu].

The ILs' purities were estimated via the area ratio[17,25,26] (Table 1) and assay (Supporting Information, S3) methods, applied on the ^{1}H NMR spectra. The reduction of anions' size reduced the ILs' purities due to thermal degradation during the roto evaporator purification. Talavera-Prieto et al. reported similar behaviors by reducing the cation size of ethanolamine-based ILs.[27] Thus, the PVA + [2HEA][Ac] and PVA + [BHEA][Ac] membranes were indeed prepared with an IL mixture instead of a pure compound.

A notable finding was the uniformly low water content in the ILs, with [m-2HEA][Pr] being the exception, exhibiting water contents below 1.1 wt %. It is important to note that the water detected is not considered a contaminant but acts as a mutual solvent for both the IL and the PVA components. Comparatively, [m-2HEA][Pr] showed a higher hygroscopic nature among the ethanolamine-based ILs. In our previous study,[21] the impact of water on CO_2 solubility within [m-2HEA][Pr] was investigated. It revealed that water concentrations at least up to approximately ∼50 wt % exert a minimal effect on CO_2 interactions. This observation suggests that increased water content does not significantly alter CO_2 absorption aside from diluting the IL. To maintain a consistent IL:PVA ratio, water contents (Table 1) were corrected on the calculus of 40 wt % of IL + PVA solution.

3.1.3. Nuclear Magnetic Resonance (NMR) Spectroscopy. Both ^{1}H and ^{13}C NMR experiments were used alongside the FT-IR to confirm all ILs' structures. On the ^{1}H NMR spectrum, the bis(2-hydroxyethyl) ammonium group was characterized by two multiplet signals at δ 3.25 and δ 3.88 assigned to the methylene hydrogens H-5 and H-6 (Figure 3a). These signals present typical chemical shifts of methylene attached to N and O, respectively. The butanoate group was characterized by one triplet at δ 2.16, with a typical chemical shift for alpha carboxyl hydrogens, one sextet at δ 1.56, and one triplet at δ 0.90, assigned to methylene H-3 and methyl H-4 hydrogens, respectively. The [BHEA][Bu] structure was also corroborated by the ^{13}C NMR spectrum (Figure 3b), by the signal at δ 186.7 assigned to the carboxylate, and by the signals at δ 42.4, δ 22.1, and δ 16.1, assigned to the methylene groups. The complete chemical shift assignments are presented in Table 2, and similar peaks and assignments were also attributed to other ethanolamine-based ILs.[17,25]

Table 2. ^{1}H and ^{13}C NMR Spectral Data for [BHEA][Bu] (D_2O at 500 and 125 MHz)[a]

Position	[BHEA][Bu] δ ^{1}H (multiplicity, J Hz)	δ ^{13}C
1	-	186.7
2	2.16 (*t*, 7.3)	42.4
3	1.56 (*sex*, 7.3)	22.1
4	0.90 (*t*, 7.3)	16.1
5;5'	3.25 (*m*)	51.7
6;6'	3.88 (*m*)	59.3

[a]*, *t* − triplet; *sex* − sextet; *m* − multiplet.

Additionally, a meticulous examination of both ^{1}H and ^{13}C NMR spectra revealed the presence of discernible signals corresponding to impurities in all samples. These impurities, however, generally accounted for less than 10 wt % of most ILs' samples (Table 2). A comparison of the principal impurity signals with the existing literature[28−32] demonstrated a resemblance in peak patterns. These previous studies ascribed these signals to an esterification reaction that occurred between the two reactants, which stems from the dehydration of carboxylic acids. Presumably, the higher charge density of smaller chain carboxylic acids, such as the acetic acid, may enhance the esterification by facilitating the engagement of the two liquid reactants to form a covalent interaction. The Supporting Information (S3) contains the HSQC and HMBC contour maps for [BHEA][Bu] and all ^{1}H and ^{13}C NMR spectra of all other six ILs studied and their assignments.

3.1.4. Fourier Transform Infrared (FT-IR) Spectroscopy. Figure 4 presents the FT-IR spectra of three ethanolamine-based ILs, and their corresponding attributions are outlined in Table 3. In the wavenumber range between 400 and 1700 cm^{-1}, more than 15 peaks were observed, complicating their precise interpretation. Nonetheless, these peaks have been associated with primary amine N−H torsion, carboxyl C−O stretch, alkyl amine C−N stretch, and secondary amine N−H

https://doi.org/10.1021/acs.iecr.3c04533
Ind. Eng. Chem. Res. 2024, 63, 8306−8318

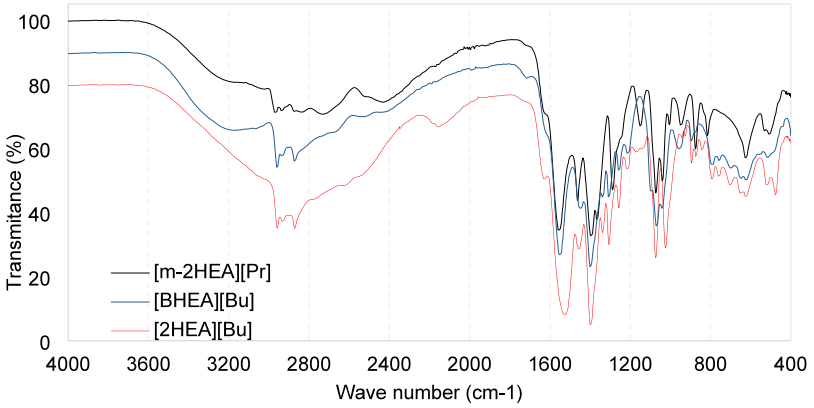

Figure 4. FT-IR spectra of [m-2HEA][Pr] (black lines), [BHEA][Bu] (blue lines)[a], and [2HEA][Bu] (red lines)[b]. [a] The transmittance of [BHEA][Bu] spectra was shifted 10% below their original values. [b] The transmittance of [2HEA][Bu] spectra was shifted 20% below their original values.

Table 3. Functional Groups Were Identified in ILs through FT-IR Analysis

wavenumber (cm^{-1})	functional group
3400−3250*	N−H stretch
3300−2500	O−H stretch of IL anion (IL anion)
3000−2850	C−H stretch
1750−1670	C═O stretch
1650−1580	N−H torsion of primary amines (IL cation)
1500−1400	symmetric and asymmetric vibrations of CH_2 and CH_3
1300−1000	C−O stretch carboxyl
1230−1030	C−N stretch of alkyl amine
910−665	N−H wag vibration of secondary amine (IL cation)

wag vibration. Absorption bands observed above a wavenumber of 2800 cm^{-1} were ascribed to the O−H and C−H vibrations. These identifications are consistent with findings reported in earlier research.[33,34]

The abundance of peaks and their overlaps present challenges in further detailed analysis of the ILs' FT-IR spectra. However, preliminary findings indicate that all ILs display analogous spectra and showcase the primary peaks anticipated based on their molecular configurations. In summary, the FT-IR results corroborate the identifications made by ^1H and ^{13}C NMR. The Supporting Information contains analogous spectra for other ILs under study (S6) and FT-IR of PVA + these ILs (S5).

3.2. Membrane Characterization. *3.2.1. ^1H NMR for PVA + IL Composite Membrane.* Figure 5A depicts the ^1H NMR spectra and a photograph of a recently prepared [m-2HEA][Pr] + PVA composite membrane. Figure 5B illustrates the ^1H NMR spectra and a photo of the same membrane following a 12 h vacuum treatment at 3 mbar and 303.15 K. Both specimens were dissolved in deuterated dimethyl sulfoxide (DMSO-d_6) before analysis.

The hydroxyl (OH) signals found on both ^1H NMR spectra, from δ 4.2 to δ 4.7, are crucial to evaluate the solvent (water) interaction with the PVA + IL membrane. The overlapped peak found on the recently synthesized membrane (Figure 5A) was attributed to water OH and PVA hydroxyl groups, indicating that the recently synthesized membrane still contained water (solvent) even after the 48 h evaporation treatment at ambient conditions. The 12 h vacuum treatment (Figure 5 B) significantly reduced this peak height, which was

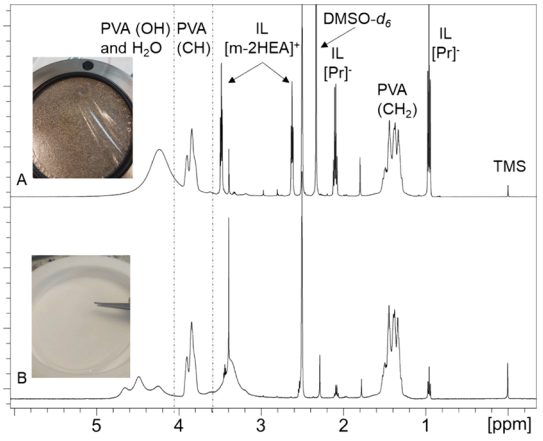

Figure 5. ^1H NMR spectrum of a PVA + [m-2HEA][Pr] recently prepared composite membrane (A) or after a 12 h vacuum treatment at 3 mbar and 303.15 K (B) (500 MHz, DMSO-d_6).

converted into signals at δ 4.65, 4.50, and 4.25, mainly attributed to PVA hydroxyl (OH). Freshly prepared PVA + [m-2HEA][Pr] presents a plastic transparent aspect, while postvacuum membranes present a stiffer aspect, similar to pure PVA membranes. The SEM images of similar PVA + [m-2HEA][Pr] membranes, performed on our previous study,[18] indicate that these materials are dense, without the formation of pores.

Signals ranging from δ 1.3 to 1.6 were further observed, identified as corresponding to the PVA's methylene groups, while the peaks around δ 3.9 ppm were associated with the polymer's CH group. These observations are consistent with the molecular structure and composition findings from a prior investigation.[35]

A comparison among the peaks of Figure 5A,B indicates that the 3 mbar vacuum treatment promoted minimal modifications of PVA-related peaks. However, those of water and [m-2HEA][Pr] were significantly reduced, indicating that the vacuum treatment promoted the expulsion of both water and IL from within the PVA matrix.

^1H NMR spectroscopy was employed to determine the concentration of [m-2HEA][Pr] in the composite membrane with PVA. Initially, the membrane preparation solution was composed of 40 wt % [m-2HEA][Pr]. However, ^1H NMR analysis of freshly prepared membrane (without additional

https://doi.org/10.1021/acs.iecr.3c04533
Ind. Eng. Chem. Res. 2024, 63, 8306−8318

treatments) indicated a reduced concentration of 32.6 wt % IL (Table 4). This reduction represents a loss of approximately

Table 4. IL Contents of the [m-2HEA][Pr] in the PVA Membrane Estimated by ^{1}H NMR

membrane	IL concentration (wt %)
freshly prepared[a]	32.6 ± 1.4[b]
30 h permeation of 2:3 (CO_2:CH_4) at 0.5 barg and 303.15 K	22.6 ± 1.0[b]
12 h exposure to 3 mbar vacuum (303.15 K)	12.3 ± 1.7[b]

[a]Without additional treatments. [b]Results as mean ± expanded uncertainty (95% with normal error distribution). All were measured in triplicates.

18.5%, equating to 7.4 wt % of the total mass, attributed to the evaporation of water during the membrane formation process. Further, exposure to a vacuum of 3 mbar at 303.15 K led to a decrease in IL content to 12.3 wt %. Additionally, prolonged exposure to a CO_2:CH_4 (40:60) gas mixture at 303.15 K and 0.5 barg resulted in the IL concentration diminishing to 22.6 wt %.

Previous research conducted by our group[18] revealed that PVA composite membranes, prepared with a 45.5 wt % [m-2HEA][Pr] solution, displayed the formation of small liquid droplets, primarily of [m-2HEA][Pr], following the solvent evaporation process. This suggests that the 40 wt % [m-2HEA][Pr] concentration used in the current study approaches the saturation point of IL in PVA. Consequently, enhancing the 32.6 wt % IL concentration within the membrane by simply increasing the [m-2HEA][Pr] concentration in the solution appears to be an ineffective approach.

3.3. Gas Permeability of [m-2HEA][Pr] + PVA Membranes. This section presents the results of a study of the performance of composite membranes for gas separation, specifically, CO_2 and CH_4. The membranes' thickness and all data on gas permeation can be found in the Supporting Information, S4.

3.3.1. IL Addition and Stream Humidification. Experimental results, depicted in Figure 6 and the Supporting Information, Tables S10-S12, evaluate the influence of IL incorporation and stream humidification on the CO_2/CH_4 separation efficiency. The addition of 32.6 wt % [m-2HEA][Pr] to the PVA matrix (sample M1) resulted in an improvement in CO_2 capture compared to the pure PVA membrane (M2). The permeability increased from 3.0 to 4.4 barrer and the selectivity increased from 2.9 to 47. Humidification of the CO_2:CH_4 (40:60) mixture further elevated the CO_2 permeability and selectivity of the PVA + [m-2HEA][Pr] membrane (M3) to 160 barrer and 106, respectively. Thus, the addition of [m-2HEA][Pr] and subsequent humidification markedly improved the CO2 permeability and CO2/CH4 selectivity by 53 and 36 times, respectively, compared to the baseline PVA membrane.

3.3.2. Transmembrane Pressure Differential and Stability. The influence of transmembrane pressure differential and stability of PVA + [m-2HEA][Pr] membranes are evaluated in Figure 7. Previous studies[19] have highlighted that the facilitated transport mechanism is likely the dominant explanation for CO_2 permeation through PVA-centric membranes. Figure 7a presents a closer look at the behavior of the CO_2 and CH_4 permeabilities of a [m-2HEA][Pr] + PVA membrane with a humidified stream (M3). The nearly constant behavior of CH_4 permeability as a function of the transmembrane pressure differential is consistent with the sorption/diffusion mechanism.[5,36] Contrastingly, the nonlinear decline of CO_2 permeability with transmembrane pressure increase suggests the presence of CO_2 facilitated transport mechanism. Deng et al.[37] correlated a similar behavior of CO_2 permeability over different transmembrane pressures to CO_2 facilitated transport mechanism.

The stability of PVA + [m-2HEA][Pr] membrane was evaluated through a ten h experiment of 2:3 CO_2/CH_4 (comprising 40% of CO_2) humidified streamflow at 303 K and 0.5 barg. Figure 7b indicates that the gas permeabilities steadily decreased over the 10 h analyzed. This effect was more pronounced on the CO_2 permeability, which decreased roughly 5.6 barrer/h, while CH_4 presented a much smaller decrease around 0.04 barrer/h. Since methane's permeability reduced more gradually than carbon dioxide's, the CO_2/CH_4 selectivity also presented a steady decrease over time. Presumably, this is a consequence of IL and water expulsion from within the membrane's matrix.

3.3.3. Temperature and CO_2:CH_4 Inlet Mol Ratio Influence. Figure 8 elucidates the effect of permeation temperature and the CO_2:CH_4 inlet mol ratio on both the CO_2 permeability and CO_2/CH_4 selectivity of [m-2HEA][Pr] + PVA membranes. As Figure 8a demonstrates, elevating the permeation temperature boosted the permeabilities of the CO_2 and the CO_2/CH_4 selectivity. Nevertheless, since the relative augmentation in CH_4 permeability exceeded that of CO_2, a resultant decrease in the CO_2/CH_4 selectivity was noted. This pattern persisted up to 333.15 K, beyond which, at temperatures surpassing 343.15 K, the membranes failed to retain stability for permeation tests.

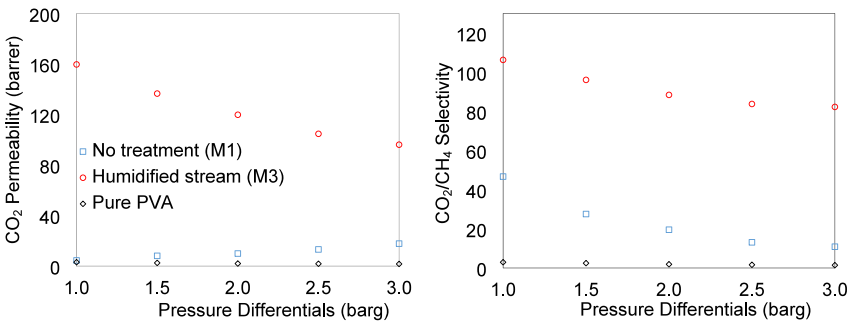

Figure 6. CO_2 Permeability (a) and selectivity to CH_4 (b) of pure PVA membrane and PVA + [m-2HEA][Pr] membranes with stream humidification (M3) and without any additional treatment (M1), at different transmembrane pressure differentials.

https://doi.org/10.1021/acs.iecr.3c04533
Ind. Eng. Chem. Res. 2024, 63, 8306−8318

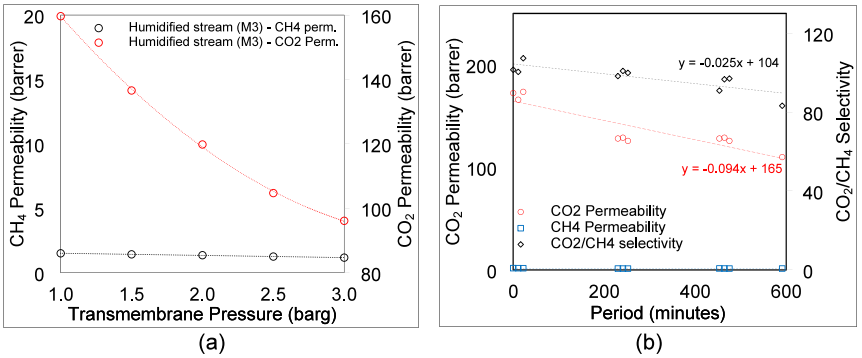

Figure 7. Humidified 2:3 CO_2:CH_4 permeation through [m-2HEA][Pr] + PVA (M3) at 303 K (a) at different transmembrane pressure differentials and (b) over membrane over longer periods of permeation, at 0.5 barg.

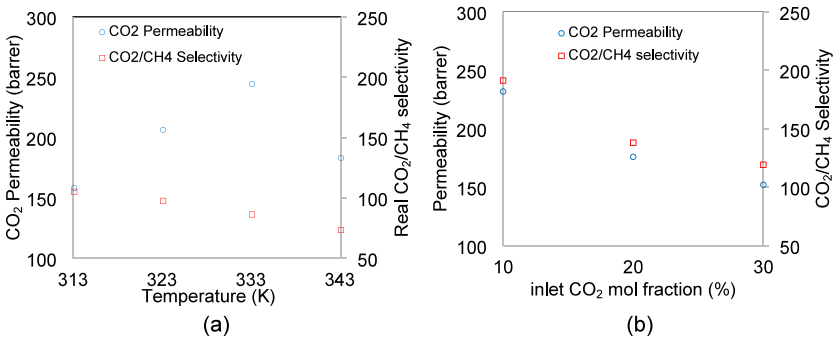

Figure 8. Effect of (a) temperature and (b) CO_2 mole fraction on the inlet stream in the CO_2 and CH_4 permeabilities of [m-2HEA][Pr] + PVA (M3) membranes at 0.5 barg.

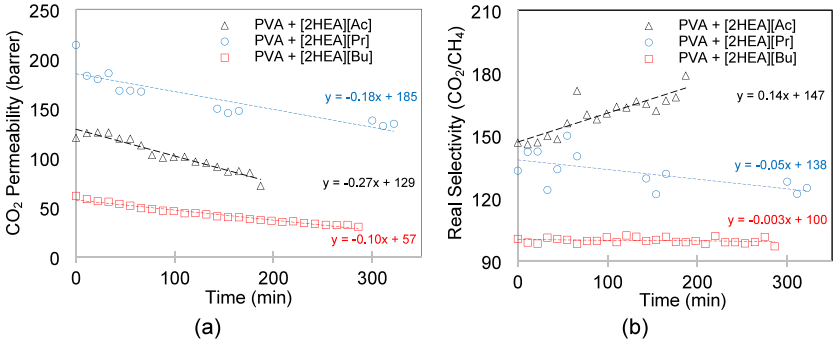

Figure 9. Permeabilities of (a) CO_2 or (b) CH_4 of IL composite membranes prepared with PVA and [2HEA][Ac], [2EHA][Pr], or [2HEA][Bu].

Given its relevance in biogas purification, a 40:60 CO_2:CH_4 ratio was predominantly chosen for this study's experiments. Nonetheless, the exploration of reduced CO_2 ratios might yield insights beneficial for industrial processes, such as the purification of natural gas or synthesis gas. Figure 8b elucidates the CO_2 permeability and CO_2/CH_4 selectivity of [m-2HEA][Pr] + PVA membranes (M3) with inlet streams containing 10, 20, and 30% of CO_2.

The data suggest that both CO_2 permeability and selectivity ascend as CO_2 concentrations in the humidified stream decline. With a 10:90 CO_2:CH_4 inlet ratio, the [m-2HEA][Pr] + PVA membranes (M3) exhibited peak CO_2 permeability and selectivity values observed in this study, recorded at 232 barrer and 191, respectively. A lower CO_2 partial pressure curtails the saturation of the CO2 carrier, bolstering the CO_2-facilitated transport mechanism, which in turn amplifies the membrane's selectivity and permeability toward this gas.

3.4. PVA + Ethanolamine-Based ILs. Motivated by the high CO_2 separation performance of [m-2HEA][Pr] + PVA membranes, six additional ethanolamine based ILs were added to PVA instead of [m-2HEA][Pr]. The combination of two ethanolamine-based cations ($[2HEA]^+$ and $[BHEA]^+$) and three carboxylic acid based anions ($[Ac]^-$, $[Pr]^-$, and $[Bu]^-$) produced the six IL investigated within this study.

3.4.1. PVA Membranes Prepared with [2HEA][R] ILs. Figure 9 shows the (a) CO_2 permeability and (b) CO_2/CH_4 selectivities of PVA membranes synthesized with [2HEA][Ac], [2HEA][Pr], and [2HEA][Bu] ionic liquids. All examined streams were subjected to a humidified mixture with 40% CO_2 under conditions of 303.15 K and 0.5 barg.

All three [2HEA][R] and PVA membranes demonstrated high CO_2/CH_4 selectivities. Notably, the [2HEA][Pr] + PVA membrane exhibited the highest CO_2 permeability at 185 barrer, while [2HEA][Ac] achieved the highest CO_2/CH_4 selectivity at 147. Consistently across all [2HEA][R]

https://doi.org/10.1021/acs.iecr.3c04533
Ind. Eng. Chem. Res. 2024, 63, 8306−8318

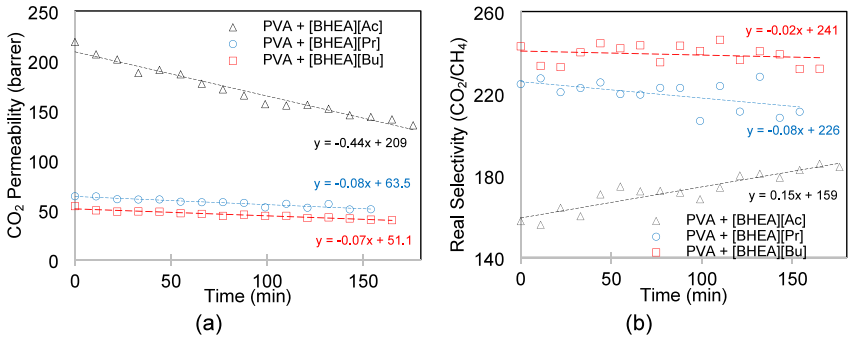

Figure 10. Permeabilities of (a) CO_2 and CO_2/CH_4 selectivities of IL composite membranes prepared with PVA and [BHEA][Ac], [BEHA][Pr], or [BHEA][Bu].

Table 5. Performance Comparison of PVA + IL Membranes Regarding Gas Permeabilities, Selectivities, and Variation over Time

IL added to PVA	CO_2 Perm. (barrer)	CO_2 Variation (barrer/h)	CH_4 Perm. (barrer)	CH_4 Variation (barrer/h)	CO_2/CH_4 Selectivity Initial	CO_2/CH_4 Selectivity Variation/h
[m-2HEA][Pr]	165	-5.6	1.58	-0.04	104	-1.5
[2HEA][Ac]	129	-16	1.34	-0.06	147	8.3
[2HEA][Pr]	185	-11	0.87	-0.14	138	-2.8
[2HEA][Bu]	57	-6.1	0.57	-0.06	100	-0.2
[BHEA][Ac]	209	-27	1.30	-0.21	159	9.1
[BHEA][Pr]	64	-4.9	0.28	-0.02	226	-4.8
[BHEA][Bu]	51	-4.2	0.21	-0.02	241	-1.2

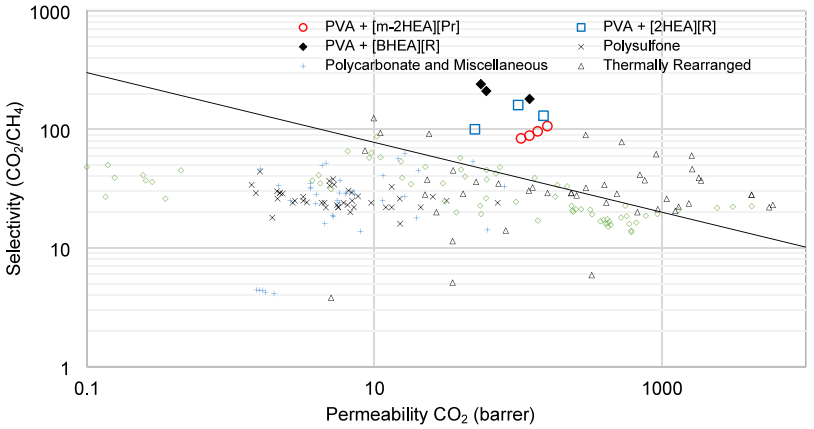

Figure 11. CO_2 permeability and CO_2/CH_4 selectivity comparison of the materials under study with the conventional materials used for membrane's CO_2 separation.

membranes, a decrease in CO_2 and CH_4 permeabilities was observed over time (Figure S21, Supporting Information S4), aligning with the behavior seen in [m-2HEA][Pr] + PVA membranes. This trend suggests that the decline in membrane performance could be linked to the expulsion of the IL with time (Table 4). Specifically, [2HEA][Ac] + PVA membranes showed a more rapid decline in CH_4 permeability compared to others, leading to an unexpected increase in CO_2/CH_4 selectivity over time.

3.4.2. PVA Membranes Prepared with [BHEA][R]-Based ILs. Incorporating [BHEA][R] ILs into the PVA matrix resulted in membranes with the highest selectivities observed in this study (Figure 10). Similar to the case for the [2HEA][R] and [m-2HEA][Pr] membranes, a gradual reduction in CO_2 and CH_4 permeability was noted over time. The [BHEA][Ac] + PVA membrane, while exhibiting the highest initial CO_2 and CH_4 permeabilities (209 and 1.3 barrer, respectively), showed the lowest CO_2/CH_4 selectivity at 159. This membrane also experienced a faster reduction in CH_4 permeability than did CO_2, leading to an increase in CO2/CH4 selectivity over time. Increasing the alkyl chain length from acetate ([Ac]) to butanoate ([Bu]) decreased the gas permeabilities but improved the CO_2/CH_4 selectivities. Among the [BHEA][R] + PVA membranes, [BHEA][Bu] displayed the highest CO_2/CH_4 selectivity at 241, while [BHEA][Ac] showed the highest CO_2 permeability at 209 barrer. The performance of [BHEA][Pr] was more balanced, closely resembling that of [BHEA][Bu].

3.4.3. Comparison of the Membranes' Performances. Table 5 summarizes the performances of ethanolamine-based IL + PVA membranes in CO_2/CH_4 separation, estimated from linear trends of gas permeabilities over time (Figures 7, 9, and 10, Figures S21 and S22, Supporting Information S4). While high CO_2 permeabilities and selectivities are preferred,

https://doi.org/10.1021/acs.iecr.3c04533
Ind. Eng. Chem. Res. 2024, 63, 8306−8318

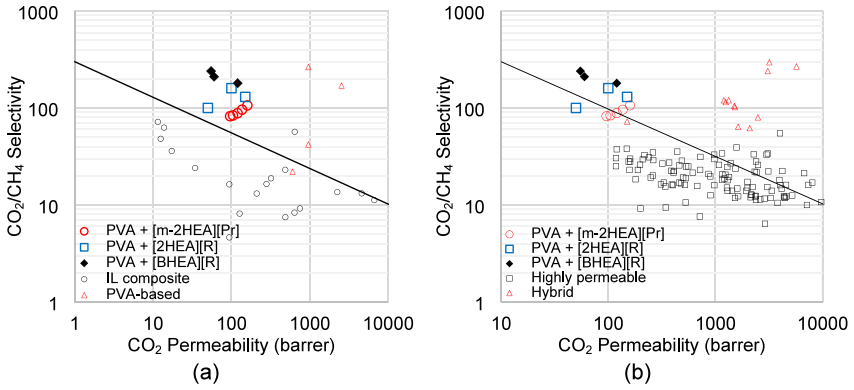

Figure 12. Comparison of CO_2 permeabilities and CO_2/CH_4 selectivities of the studied membranes with (a) IL composite polymer membranes and (b) highly permeable and hybrid membranes.

negative variations are undesirable due to stability concerns, especially regarding the CO_2 permeability over time. Membranes formed with [m-2HEA][Pr] and [2HEA][Pr] emerged as the most promising materials, offering high CO_2 permeabilities at 165 and 185 barrer, respectively. [BHEA]-[Bu] membranes achieved the highest CO_2/CH_4 selectivity and demonstrated the least variation over time, indicating superior stability with values reaching 241 and a change rate of −4.2 barrer/h, respectively.

A correlation exists between the IL anions' alkyl chain length and membrane performance: extending the chain from acetate ([Ac]) to butanoate ([Bu]) reduces gas permeabilities and enhances CO_2/CH_4 selectivities. However, ILs with acetate anions showed higher CH_4 permeabilities and greater instability, making them less suitable for the CO_2/CH_4 separation despite their higher permeation potential. Overall, bis-2-hydroxyethylammonium ([BHEA][R]) IL composite membranes yielded higher selectivities, while monodentate *N*-2-hydroxyethylammonium ([2HEA][R]) ILs led to membranes with superior permeabilities.

Figure 11 provides a comparison of the CO_2 separation performance of the studied membranes with some of the literature's membranes with the highest performance for CO_2/CH_4 separation. The comparison suggests that the studied IL composite membranes exhibited outstanding CO_2/CH_4 selectivities and moderate CO_2 permeabilities compared to a majority of conventional sorption-diffusion polymeric membranes. The compared membranes include those made of polyimide[38−45] (represented by green diamonds), polysulfone[46−57] (represented by black x), thermally rearranged polymers (TR)[58−62] (represented by black triangles), and polycarbonates and various polymers[63−78] (represented by blue crosses).

Figure 12a contrasts the performance of the membranes under study with other IL composite membranes[7] and distinct PVA-based materials.[3,19] The studied ethanolamine-based ILs produced higher CO_2/CH_4 selectivities than all of the IL composite membranes reported in the open literature. The comparison with other PVA based membranes indicates that the studied membranes presented significantly lower CO_2 permeabilities. Thus, it indicates gaps for the development of IL composite membranes with other PVA-based materials. For instance, PVA is amalgamated with CO_2-facilitated transport polymers like PVAm,[37] which amplifies CO_2 separation efficiency, albeit potentially compromising the membrane's structural integrity.

Given that gas permeation poses a significant challenge for industrial gas separation using membranes, Figure 12b was dedicated to comparing the materials under study with the most promising high-permeability membranes recently cited in the academic literature.[3] The PVA + ethanolamine-based membranes notably surpassed most in terms of CO_2/CH_4 selectivity, except for some hybrid materials, including a few that are IL-based.

This study's findings indicate that the ethanolamine-based ILs + PVA membrane produced materials with high CO_2/CH_4 selectivity, however, associated with low stability. Gaps for the increase in the CO_2 permeability were found by comparison with similar materials studied in the open literature. Incorporating solid particles, such as ZnO, silica, or alumina, has been cited to boost the CO_2 permeability. Furthermore, blended PVA polymers were reported to produce significantly higher CO_2 permeabilities than those of pure polymers. The addition of materials such as PVAm, PEI, and PAMAM could produce promising materials.

CONCLUSIONS

This study evaluated the use of ethanolamine based ILs and PVA membranes for CO_2/CH_4 separation. The ILs' chemical structures and purity were determined using FTIR, Karl Fischer titrator, ^1H, and ^{13}C NMR. Analyses indicate the IL synthesis produced few impurities and water content. NMR analyses of PVA + 40 wt % of [m-2HEA][Pr] membranes indicate that part of the IL is lost during solvent evaporation (7.4 wt % loss). Vacuum 3 mbar vacuum treatment and 10h gas flow further reduced the IL concentration from within the IL composite membrane, reaching 22.6 and 12.3 wt %, respectively.

The incorporation of 32.6 wt % of [m-2HEA][Pr] to PVA matrix and humidification of mixed CO_2:CH_4 (40:60) stream promoted an outstanding increase of both CO_2 permeability (53 times) and CO_2/CH_4 selectivity (36 times). While pure PVA membrane presented CO_2 permeability and selectivity of 3.0 barrer and 2.9, PVA + 32.6 wt % of [m-2HEA][Pr] presented 160 barrer and 106, respectively.

The temperature increase enhanced CO_2 and CH_4 permeabilities up to 333 K, while low CO_2 partial pressures increased both the CO_2 permeability and selectivity. The nearly exponential behavior of CO_2 permeability and selectivity at low transmembrane pressure differentials suggest the occurrence of CO_2 facilitated transport mechanism. Both CO_2 and CH_4 presented a steady reduction of permeability

https://doi.org/10.1021/acs.iecr.3c04533
Ind. Eng. Chem. Res. 2024, 63, 8306−8318

over time. This instability was attributed to the reduction of IL concentration over time.

Six different ethanolamine-based ILs were added to the PVA matrix. An increase in the alkyl chain length of ILs' anion, from acetate [Ac] to butanoate [Bu], produced membranes with moderate CO_2 permeabilities, and high CO_2/CH_4 selectivities and stabilities. Bidentade bis-2-hydroxyethylammonium ILs [BHEA][R] produced membranes with higher selectivities, while monodentate *N*-2-hydroxyethylammonium ILs [2HEA]-[R], promoted a CO_2 permeability increase.

The most promising membranes for higher CO_2 permeability applications were [m-2HEA][Pr] and [2HEA][Pr] (165 and 185 barrer, respectively). Meanwhile, [BHEA][Bu] produced membranes with the highest CO_2/CH_4 selectivity and lowest variation over time (highest stability), reaching 241 and −4.2 barrer/h, respectively.

The comparison of the CO_2/CH_4 separation performance to other promising CO_2 separation membranes indicates that ethanolamine-based ILs + PVA's major advantages are their outstanding CO_2/CH_4 selectivities while maintaining moderate CO_2 permeabilities.

The development of this material for CO_2 separation purposes would benefit from studies addressing the IL loss issue over long periods, increase of CO_2 permeability, or blending ethanolamine-based ILs to other materials to leverage their high CO_2/CH_4 selectivities.

■ ASSOCIATED CONTENT

Supporting Information

The Supporting Information is available free of charge at https://pubs.acs.org/doi/10.1021/acs.iecr.3c04533.

(S7) IL_FTIR_data (XLSX)

(S1) Materials, suppliers, purities, and molecular structures; (S2) calculation of water vapor content in a saturated gaseous system; (S3) NMR spectra; (S4) membrane thickness and gas permeation experiments; (S5) FT-IR of membranes; (S6) charge density distributions and sigma-profile (PDF)

■ AUTHOR INFORMATION

Corresponding Author

Murilo Leite Alcantara − *Department of Chemical Engineering, Federal University of Bahia, Salvador, BA 40210-630, Brazil; Department of Chemical Engineering, University of São Paulo, 05508-070 São Paulo, Brazil; CICECO − Aveiro Institute of Materials, Department of Chemistry, University of Aveiro, Aveiro 3810-1933, Portugal;* orcid.org/0000-0002-4312-1836; Email: murilo.la@ua.pt

Authors

Gerlon de Almeida Ribeiro Oliveira − *Department of Pharmacy, Health Sciences School, University of Brasília, Brasília, DF 70910-900, Brazil; NMR Laboratory, Institute of Chemistry, Federal University of Goiás, Goiânia, GO 74690-900, Brazil*

Luciano Morais Lião − *NMR Laboratory, Institute of Chemistry, Federal University of Goiás, Goiânia, GO 74690-900, Brazil;* orcid.org/0000-0001-9985-2980

Alfredo Ortiz − *Department of Chemical & Biomolecular Engineering, University of Cantábria, Santander, CA 39005, Spain*

Silvana Mattedi − *Department of Chemical Engineering, Federal University of Bahia, Salvador, BA 40210-630, Brazil;* orcid.org/0000-0003-4816-7494

Complete contact information is available at: https://pubs.acs.org/10.1021/acs.iecr.3c04533

Notes

The authors declare no competing financial interest.

M.L.A. performed conceptualization, methodology, formal analysis, investigation, writing − original draft; S.M. performed conceptualization, investigation, resource gathering, supervision, and manuscript review. G.A.R.O. did the methodology, NMR data analyses, and writing; L.M.L. performed resource gathering, NMR data analyses, and manuscript review; A.O. performed conceptualization, resource gathering, supervision, and review.

■ ACKNOWLEDGMENTS

The authors gratefully acknowledge the support from FAPESB (Project APP0075/2016), CAPES (Coordination for the Improvement of Higher Education Personnel)/Brazil (PDSE-88881.132805/2016-01), process no. 2021/07155-6, Research Support Foundation of the State of São Paulo (FAPESP) and, National Council for Scientific and Technological Development/Brazil (CNPq) (grant PQ-311342/2022-1 for S.M. and PQ-310051/2022-3 for L.M.L.). Grammarly and Chat GPT 4.0 tools were used herein to correct grammar and increase the readability of the original manuscript. The prompt used on chat GPT 4.0 was the following: "Correct the grammar and increase the readability of this academic manuscript. Do not perform any additional modification, nor add or modify any information on the original manuscript. Maintain the original meaning."

■ REFERENCES

(1) ESRL, N. E. S. R. L. *Trends in Atmospheric Carbon Dioxide.* https://www.esrl.noaa.gov/gmd/ccgg/trends/gl_trend.html (accessed 2021−01−13).

(2) Leclaire, J.; Heldebrant, D. J. A Call to (Green) Arms: A Rallying Cry for Green Chemistry and Engineering for CO 2 Capture, Utilisation and Storage. *Green Chem.* **2018**, *20* (22), 5058−5081.

(3) Wang, S.; Li, X.; Wu, H.; Tian, Z.; Xin, Q.; He, G.; Peng, D.; Chen, S.; Yin, Y.; Jiang, Z.; Guiver, M. D. Advances in High Permeability Polymer-Based Membrane Materials for CO 2 Separations. *Energy Environ. Sci.* **2016**, *9* (6), 1863−1890.

(4) Dai, Z.; Noble, R. D.; Gin, D. L.; Zhang, X.; Deng, L. Combination of Ionic Liquids with Membrane Technology: A New Approach for CO 2 Separation. *J. Membr. Sci.* **2016**, *497*, 1−20.

(5) Baker, R. W. *Membrane Technology and Applications*, 2nd ed.; Sons, J. W. &, Ed.; John Wiley & Sons: Chichester, Englaterra, 2004.

(6) Friess, K.; Izák, P.; Kárászová, M.; Pasichnyk, M.; Lanč, M.; Nikolaeva, D.; Luis, P.; Jansen, J. C. A Review on Ionic Liquid Gas Separation Membranes. *Membranes (Basel)* **2021**, *11* (2), 97.

(7) Yan, X.; Anguille, S.; Bendahan, M.; Moulin, P. Ionic Liquids Combined with Membrane Separation Processes: A Review. *Sep Purif Technol.* **2019**, *222* (March), 230−253.

(8) Fam, W.; Mansouri, J.; Li, H.; Chen, V. Improving CO2 Separation Performance of Thin Film Composite Hollow Fiber with Pebax®1657/Ionic Liquid Gel Membranes. *J. Membr. Sci.* **2017**, *537*, 54−68.

(9) Klemm, A.; Lee, Y. Y.; Mao, H.; Gurkan, B. Facilitated Transport Membranes With Ionic Liquids for CO2 Separations. *Front. Chem.* **2020**, *8* (August), 1−8.

(10) Marsh, K. N.; Boxall, J. A.; Lichtenthaler, R. Room Temperature Ionic Liquids and Their Mixtures - A Review. *Fluid Phase Equilib.* **2004**, *219* (1), 93−98.
(11) Carvalho, P. J.; Kurnia, K. A.; Coutinho, J. A. P. Dispelling Some Myths about the CO 2 Solubility in Ionic Liquids. *Phys. Chem. Chem. Phys.* **2016**, *18* (22), 14757−14771.
(12) Hospital-Benito, D.; Lemus, J.; Moya, C.; Santiago, R.; Palomar, J. Process Analysis Overview of Ionic Liquids on CO2 Chemical Capture. *Chemical Engineering Journal* **2020**, *390*, No. 124509.
(13) Latała, A.; Nędzi, M.; Stepnowski, P. Toxicity of Imidazolium Ionic Liquids towards Algae. Influence of Salinity Variations. *Green Chem.* **2010**, *12* (1), 60−64.
(14) George, A.; Brandt, A.; Tran, K.; Zahari, S. M. S. N. S.; Klein-Marcuschamer, D.; Sun, N.; Sathitsuksanoh, N.; Shi, J.; Stavila, V.; Parthasarathi, R.; Singh, S.; Holmes, B. M.; Welton, T.; Simmons, B. a.; Hallett, J. P. Design of Low-Cost Ionic Liquids for Lignocellulosic Biomass Pretreatment. *Green Chem.* **2015**, *17* (3), 1728−1734.
(15) Peric, B. *Evaluation of (Eco) Toxicity and Biodegradability of Short Aliphatic Protic Ionic Liquids*; Universitat de Barcelona 2014.
(16) Ur Rehman, R.; Rafiq, S.; Muhammad, N.; Khan, A. L.; Ur Rehman, A.; TingTing, L.; Saeed, M.; Jamil, F.; Ghauri, M.; Gu, X. Development of Ethanolamine-Based Ionic Liquid Membranes for Efficient CO 2 /CH 4 Separation. *J. Appl. Polym. Sci.* **2017**, *134* (44), 45395.
(17) Alcantara, M. L.; Ferreira, P. I. S.; Pisoni, G. O.; Silva, A. K.; Cardozo-Filho, L.; Lião, L. M.; Pires, C. A. M.; Mattedi, S. High Pressure Vapor-Liquid Equilibria for Binary Protic Ionic Liquids + Methane or Carbon Dioxide. *Sep. Purif. Technol.* **2018**, *196* (March 2017), 32−40.
(18) Alcantara, M. L.; de Almeida Oliveira, G.; Lião, L. M.; Borges, C. P.; Mattedi, S. Amine/Carboxylic Acid Ionic Liquid Composite Membranes for CO2 Separation. *Ind. Eng. Chem. Res.* **2021**, *60* (11), 4405−4419.
(19) Hong, C.-H.; Ahmad, N. N. R.; Leo, C. P.; Ahmad, A. L.; Mohammad, A. W. Progress in Polyvinyl Alcohol Membranes with Facilitated Transport Properties for Carbon Capture. *J. Environ. Chem. Eng.* **2021**, *9*, No. 106783.
(20) Ferrarini, F.; Flôres, G. B.; Muniz, A. R.; de Soares, R. P. An Open and Extensible Sigma-profile Database for COSMO-based Models. *AIChE J.* **2018**, *64* (9), 3443−3455.
(21) Alcantara, M. L.; Silva, P. H. R.; Romanielo, L. L.; Cardozo-Filho, L.; Mattedi, S. Effect of Water on High-Pressure Ternary Phase Equilibria of CO2 + H2O + Alkanolamine Based Ionic Liquid. *J. Mol. Liq.* **2020**, *306*, No. 112775.
(22) Malz, F. Quantitative NMR in the Solution State NMR. In *NMR Spectroscopy in Pharmaceutical Analysis*; Elsevier, 2008; pp 43−62. DOI: 10.1016/B978-0-444-53173-5.00002-0.
(23) Pauli, G. F.; Gödecke, T.; Jaki, B. U.; Lankin, D. C. Quantitative 1 H NMR. Development and Potential of an Analytical Method: An Update. *J. Nat. Prod* **2012**, *75* (4), 834−851.
(24) Aparicio, S.; Atilhan, M.; Khraisheh, M.; Alcalde, R. Study on Hydroxylammonium-Based Ionic Liquids. *I. Characterization. J. Phys. Chem. B* **2011**, *115* (43), 12473−12486.
(25) Alcantara, M. L.; de Carvalho, M. L.; Álvarez, V. H.; Ferreira, P. I. S.; Paredes, M. L. L.; Cardozo-Filho, L.; Silva, A. K.; Lião, L. M.; Pires, C. A. M.; Mattedi, S. High Pressure Vapor-Liquid Equilibria for Binary Carbon Dioxide and Protic Ionic Liquid Based on Ethanolamines + Butanoic Acid. *Fluid Phase Equilib.* **2018**, *460*, 162−174.
(26) Alcantara, M. L.; Santos, J. P.; Loreno, M.; Ferreira, P. I. S.; Paredes, M. L. L.; Cardozo-Filho, L.; Silva, A. K.; Lião, L. M.; Pires, C. A. M.; Mattedi, S. Low Viscosity Protic Ionic Liquid for CO2/CH4 Separation: Thermophysical and High-Pressure Phase Equilibria for Diethylammonium Butanoate. *Fluid Phase Equilib.* **2018**, *459*, 30−43.
(27) Talavera-Prieto, N. M. C. C.; Ferreira, A. G. M. M.; Simões, P. N.; Carvalho, P. J.; Mattedi, S.; Coutinho, J. A. P. P. Thermophysical Characterization of N-Methyl-2-Hydroxyethylammonium Carboxilate Ionic Liquids. *J. Chem. Thermodyn* **2014**, *68* (3), 221−234.
(28) Florindo, C.; Oliveira, F. S.; Rebelo, L. P. N.; Fernandes, A. M.; Marrucho, I. M. Insights into the Synthesis and Properties of Deep Eutectic Solvents Based on Cholinium Chloride and Carboxylic Acids. *ACS Sustain Chem. Eng.* **2014**, *2* (10), 2416−2425.
(29) CHEN, W.; XUE, Z.; WANG, J.; JIANG, J.; ZHAO, X.; MU, T. Investigation on the Thermal Stability of Deep Eutectic Solvents. *Acta Physico-Chimica Sinica* **2018**, *34* (8), 904−911.
(30) Abbott, A. P.; Boothby, D.; Capper, G.; Davies, D. L.; Rasheed, R. K. Deep Eutectic Solvents Formed between Choline Chloride and Carboxylic Acids: Versatile Alternatives to Ionic Liquids. *J. Am. Chem. Soc.* **2004**, *126* (29), 9142−9147.
(31) Rodriguez Rodriguez, N.; van den Bruinhorst, A.; Kollau, L. J. B. M.; Kroon, M. C.; Binnemans, K. Degradation of Deep-Eutectic Solvents Based on Choline Chloride and Carboxylic Acids. *ACS Sustain Chem. Eng.* **2019**, *7* (13), 11521−11528.
(32) Francisco, M.; van den Bruinhorst, A.; Kroon, M. C. Low-Transition-Temperature Mixtures (LTTMs): A New Generation of Designer Solvents. *Angew. Chem., Int. Ed.* **2013**, *52* (11), 3074−3085.
(33) Álvarez, V. H.; Dosil, N.; Gonzalez-Cabaleiro, R.; Mattedi, S.; Martin-Pastor, M.; Iglesias, M.; Navaza, J. M. Brønsted Ionic Liquids for Sustainable Processes: Synthesis and Physical Properties. *J. Chem. Eng. Data* **2010**, *55* (2), 625−632.
(34) Lopes, W. A.; Fascio, M. Esquema Para Interpretação de Espectros de Substâncias Orgânicas Na Região Do Infravermelho. *Quim. Nova* **2004**, *27* (4), 670−673.
(35) Korbag, I.; Mohamed Saleh, S. Studies on the Formation of Intermolecular Interactions and Structural Characterization of Polyvinyl Alcohol/Lignin Film. *International Journal of Environmental Studies* **2016**, *73* (2), 226−235.
(36) Matsuyama, H.; Terada, A.; Nakagawara, T.; Kitamura, Y.; Teramoto, M. Facilitated Transport of CO2 through Polyethylenimine/Poly(Vinyl Alcohol) Blend Membrane. *J. Membr. Sci.* **1999**, *163* (2), 221−227.
(37) Deng, L.; Kim, T.-J.; Hägg, M.-B. Facilitated Transport of CO2 in Novel PVAm/PVA Blend Membrane. *J. Membr. Sci.* **2009**, *340* (1−2), 154−163.
(38) White, L. S.; Blinka, T. A.; Kloczewski, H. A.; Wang, I. Properties of a Polyimide Gas Separation Membrane in Natural Gas Streams. *J. Membr. Sci.* **1995**, *103* (1−2), 73−82.
(39) Ayala, D. Gas Separation Properties of Aromatic Polyimides. *J. Membr. Sci.* **2003**, *215* (1−2), 61−73.
(40) Xiao, Y.; Chung, T.; Guan, H.; Guiver, M. Synthesis, Cross-Linking and Carbonization of Co-Polyimides Containing Internal Acetylene Units for Gas Separation. *J. Membr. Sci.* **2007**, *302* (1−2), 254−264.
(41) Chan, S. S.; Chung, T.-S.; Liu, Y.; Wang, R. Gas and Hydrocarbon (C2 and C3) Transport Properties of Co-Polyimides Synthesized from 6FDA and 1,5-NDA (Naphthalene)/Durene Diamines. *J. Membr. Sci.* **2003**, *218* (1−2), 235−245.
(42) Staudt-Bickel, C.; Koros, J. W. Improvement of CO2/CH4 Separation Characteristics of Polyimides by Chemical Crosslinking. *J. Membr. Sci.* **1999**, *155* (1), 145−154.
(43) Peter, J.; Khalyavina, A.; Kříž, J.; Bleha, M. Synthesis and Gas Transport Properties of ODPA−TAP−ODA Hyperbranched Polyimides with Various Comonomer Ratios. *Eur. Polym. J.* **2009**, *45* (6), 1716−1727.
(44) Wang, L.; Cao, Y.; Zhou, M.; Zhou, S. J.; Yuan, Q. Novel Copolyimide Membranes for Gas Separation. *J. Membr. Sci.* **2007**, *305* (1−2), 338−346.
(45) Hillock, A. M. W.; Koros, W. J. Cross-Linkable Polyimide Membrane for Natural Gas Purification and Carbon Dioxide Plasticization Reduction. *Macromolecules* **2007**, *40* (3), 583−587.
(46) Kim, H.-J.; Hong, S.-I. The Sorption and Permeation of Co2 and Ch4 for Dimethylated Polysulfone Membrane. *Korean Journal of Chemical Engineering* **1997**, *14* (3), 168−174.
(47) Ghosal, K.; Chern, R. T.; Freeman, B. D.; Daly, W. H.; Negulescu, I. I. Effect of Basic Substituents on Gas Sorption and Permeation in Polysulfone. *Macromolecules* **1996**, *29* (12), 4360−4369.

https://doi.org/10.1021/acs.iecr.3c04533
Ind. Eng. Chem. Res. 2024, 63, 8306−8318

(48) McHattie, J. S.; Koros, W. J.; Paul, D. R. Gas Transport Properties of Polysulphones: 1. Role of Symmetry of Methyl Group Placement on Bisphenol Rings. *Polymer (Guildf)* **1991**, *32* (5), 840−850.
(49) McHattie, J. S.; Koros, W. J.; Paul, D. R. Gas Transport Properties of Polysulphones: 2. Effect of Bisphenol Connector Groups. *Polymer (Guildf)* **1991**, *32* (14), 2618−2625.
(50) McHattie, J. S.; Koros, W. J.; Paul, D. R. Gas Transport Properties of Polysulphones: 3. Comparison of Tetramethyl-Substituted Bisphenols. *Polymer (Guildf)* **1992**, *33* (8), 1701−1711.
(51) Aitken, C. L.; Koros, W. J.; Paul, D. R. Effect of Structural Symmetry on Gas Transport Properties of Polysulfones. *Macromolecules* **1992**, *25* (13), 3424−3434.
(52) Pixton, M. R.; Paul, D. R. Gas Transport Properties of Adamantane-Based Polysulfones. *Polymer (Guildf)* **1995**, *36* (16), 3165−3172.
(53) Jomekian, A.; Mansoori, S. A. A.; Monirimanesh, N.; Shafiee, A. Gas Transport Behavior of DMDCS Modified MCM-48/Polysulfone Mixed Matrix Membrane Coated by PDMS. *Korean Journal of Chemical Engineering* **2011**, *28* (10), 2069−2075.
(54) Camacho-Zuñiga, C.; Ruiz-Treviño, F. A.; Hernández-López, S.; Zolotukhin, M. G.; Maurer, F. H. J.; González-Montiel, A. Aromatic Polysulfone Copolymers for Gas Separation Membrane Applications. *J. Membr. Sci.* **2009**, *340* (1−2), 221−226.
(55) Kim, H.-J.; Hong, S.-I. The Transport Properties of CO2 and CH4 for Brominated Polysulfone Membrane. *Korean Journal of Chemical Engineering* **1999**, *16* (3), 343−350.
(56) Houde, A. Y.; Kulkarni, S. S.; Kulkarni, M. G. Sorption, Transport, and History Effects in Phenolphthalein-Based Polysulfone. *J. Membr. Sci.* **1994**, *95* (2), 147−160.
(57) Ghosal, K.; Chern, R. T. Aryl-Nitration of Poly(Phenylene Oxide) and Polysulfone. *J. Membr. Sci.* **1992**, *72* (1), 91−97.
(58) Li, S.; Jo, H. J.; Han, S. H.; Park, C. H.; Kim, S.; Budd, P. M.; Lee, Y. M. Mechanically Robust Thermally Rearranged (TR) Polymer Membranes with Spirobisindane for Gas Separation. *J. Membr. Sci.* **2013**, *434*, 137−147.
(59) Park, H. B.; Jung, C. H.; Lee, Y. M.; Hill, A. J.; Pas, S. J.; Mudie, S. T.; Van Wagner, E.; Freeman, B. D.; Cookson, D. J. Polymers with Cavities Tuned for Fast Selective Transport of Small Molecules and Ions. *Science (1979)* **2007**, *318* (5848), 254−258.
(60) Yeong, Y. F.; Wang, H.; Pallathadka Pramoda, K.; Chung, T.-S. Thermal Induced Structural Rearrangement of Cardo-Copolybenzoxazole Membranes for Enhanced Gas Transport Properties. *J. Membr. Sci.* **2012**, *397*−*398*, 51−65.
(61) Calle, M.; Lee, Y. M. Thermally Rearranged (TR) Poly(Ether−benzoxazole) Membranes for Gas Separation. *Macromolecules* **2011**, *44* (5), 1156−1165.
(62) Choi, J. I.; Jung, C. H.; Han, S. H.; Park, H. B.; Lee, Y. M. Thermally Rearranged (TR) Poly(Benzoxazole-Co-Pyrrolone) Membranes Tuned for High Gas Permeability and Selectivity. *J. Membr. Sci.* **2010**, *349* (1−2), 358−368.
(63) Chan, A. H.; Koros, W. J.; Paul, D. R. Analysis of Hydrocarbon Gas Sorption and Transport in Ethyl Cellulose Using the Dual Sorption/Partial Immobilization Models. *J. Membr. Sci.* **1978**, *3* (2), 117−130.
(64) Rajabi, Z.; Moghadassi, A. R.; Hosseini, S. M.; Mohammadi, M. Preparation and Characterization of Polyvinylchloride Based Mixed Matrix Membrane Filled with Multi Walled Carbon Nano Tubes for Carbon Dioxide Separation. *Journal of Industrial and Engineering Chemistry* **2013**, *19* (1), 347−352.
(65) Barbari, T. A.; Koros, W. J.; Paul, D. R. Polymeric Membranes Based on Bisphenol-A for Gas Separations. *J. Membr. Sci.* **1989**, *42* (1−2), 69−86.
(66) Barrer, R. M. Diffusivities in Glassy Polymers for the Dual Mode Sorption Model. *J. Membr. Sci.* **1984**, *18*, 25−35.
(67) Adams, R. T.; Lee, J. S.; Bae, T.-H.; Ward, J. K.; Johnson, J. R.; Jones, C. W.; Nair, S.; Koros, W. J. CO2−CH4 Permeation in High Zeolite 4A Loading Mixed Matrix Membranes. *J. Membr. Sci.* **2011**, *367* (1−2), 197−203.
(68) Xing, R.; Ho, W. S. W. Synthesis and Characterization of Crosslinked Polyvinylalcohol/Polyethyleneglycol Blend Membranes for CO2/CH4 Separation. *J. Taiwan Inst Chem. Eng.* **2009**, *40* (6), 654−662.
(69) Weng, T.-H.; Tseng, H.-H.; Wey, M.-Y. Effect of SBA-15 Texture on the Gas Separation Characteristics of SBA-15/Polymer Multilayer Mixed Matrix Membrane. *J. Membr. Sci.* **2011**, *369* (1−2), 550−559.
(70) Perez, E. V.; Balkus, K. J.; Ferraris, J. P.; Musselman, I. H. Mixed-Matrix Membranes Containing MOF-5 for Gas Separations. *J. Membr. Sci.* **2009**, *328* (1−2), 165−173.
(71) Moghadam, F.; Omidkhah, M. R.; Vasheghani-Farahani, E.; Pedram, M. Z.; Dorosti, F. The Effect of TiO2 Nanoparticles on Gas Transport Properties of Matrimid5218-Based Mixed Matrix Membranes. *Sep Purif Technol.* **2011**, *77* (1), 128−136.
(72) Castro-Muñoz, R.; Fíla, V. Progress on Incorporating Zeolites in Matrimid®5218 Mixed Matrix Membranes towards Gas Separation. *Membranes (Basel)* **2018**, *8* (2), 30.
(73) Ahn, J.; Chung, W.-J.; Pinnau, I.; Guiver, M. D. Polysulfone/Silica Nanoparticle Mixed-Matrix Membranes for Gas Separation. *J. Membr. Sci.* **2008**, *314* (1−2), 123−133.
(74) Kim, S.; Chen, L.; Johnson, J. K.; Marand, E. Polysulfone and Functionalized Carbon Nanotube Mixed Matrix Membranes for Gas Separation: Theory and Experiment. *J. Membr. Sci.* **2007**, *294* (1−2), 147−158.
(75) Dorosti, F.; Omidkhah, M. R.; Pedram, M. Z.; Moghadam, F. Fabrication and Characterization of Polysulfone/Polyimide−Zeolite Mixed Matrix Membrane for Gas Separation. *Chemical Engineering Journal* **2011**, *171* (3), 1469−1476.
(76) Kim, S.; Marand, E. High Permeability Nano-Composite Membranes Based on Mesoporous MCM-41 Nanoparticles in a Polysulfone Matrix. *Microporous Mesoporous Mater.* **2008**, *114* (1−3), 129−136.
(77) Cakal, U.; Yilmaz, L.; Kalipcilar, H. Effect of Feed Gas Composition on the Separation of CO2/CH4Mixtures by PES-SAPO 34-HMA Mixed Matrix Membranes. *J. Membr. Sci.* **2012**, *417*−*418*, 45−51.
(78) Ismail, A.; Kusworo, T.; Mustafa, A. Enhanced Gas Permeation Performance of Polyethersulfone Mixed Matrix Hollow Fiber Membranes Using Novel Dynasylan Ameo Silane Agent. *J. Membr. Sci.* **2008**, *319* (1−2), 306−312.

https://doi.org/10.1021/acs.iecr.3c04533
Ind. Eng. Chem. Res. 2024, 63, 8306−8318